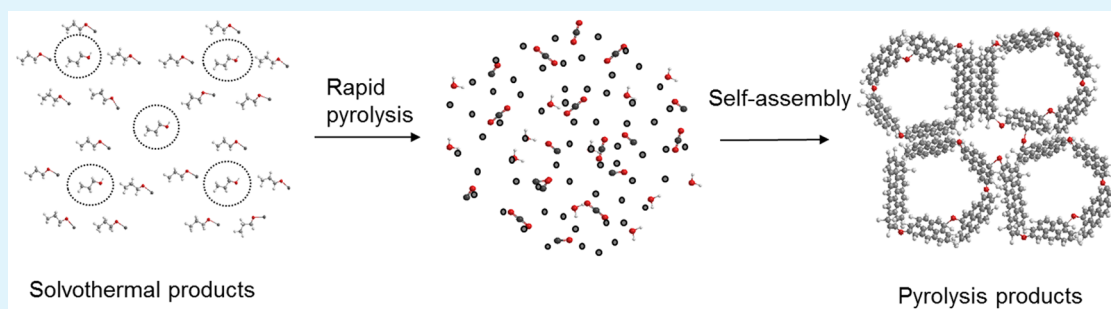# Understanding the Formation Mechanism of Graphene Frameworks Synthesized by Solvothermal and Rapid Pyrolytic Processes Based on an Alcohol−Sodium Hydroxide System

Huijuan Cui,[†,‡] Jianfeng Zheng,*[,†] Pengju Yang,[†,‡] Yanyan Zhu,[†,‡] Zhijian Wang,[†] and Zhenping Zhu*[,†]

[†]State Key Laboratory of Coal Conversion, Institute of Coal Chemistry, Chinese Academy of Sciences, Taiyuan, 030001 China
[‡]University of Chinese Academy of Sciences, Beijing, 010049 China

Ⓢ *Supporting Information*

ABSTRACT: The determination of ways to facilitate the 2D-oriented assembly of carbons into graphene instead of other carbon structures while restraining the $\pi-\pi$ stacking interaction is a challenge for the controllable bulk synthesis of graphene, which is vital both scientifically and technically. In this study, graphene frameworks (GFs) are synthesized by solvothermal and rapid pyrolytic processes based on an alcohol−sodium hydroxide system. The evolution mechanism of GFs is investigated systematically. Under sodium catalysis, the abundant carbon atoms produced by the fast decomposition of solvothermal intermediate self-assembled to graphene. The existence of abundant ether bonds may be favorable for 3D graphene formation. More importantly, GFs were successfully obtained using acetic acid as the carbon source in the synthetic process, suggesting the reasonability of analyzing the formation mechanism. It is quite possible to determine more favorable routes to synthesize graphene under this cognition. The electrochemical energy storage capacity of GFs was also studied, which revealed a high supercapacitor performance with a specific capacitance of 310.7 F/g at the current density of 0.2 A/g.

KEYWORDS: graphene, alcohol−sodium, formation mechanism, solvothermal, pyrolysis

■ INTRODUCTION

Graphene, an emerging structure of free-standing carbon atoms packed into a dense honeycomb crystal structure, has elicited considerable interest because of its fascinating properties and great potential applications.[1−6] However, large-scale graphene preparation remains challenging because of its inability to effectively inhibit stacking together under strong $\pi-\pi$ interaction to form thick graphite crystals or curve up, driven by the stabilization of the peripheral dangling bonds to form curved structures (e.g., carbon nanotubes, fullerenes, and even amorphous carbons).[7−11] Although a top-down strategy, especially for exfoliating graphite oxidation, has been considered as a possible method of bulk preparation, the basic electric properties of graphene are usually lost because of the damage of the $\pi-\pi$-conjugated structure during oxidation.[1,12] Bottom-up assembly strategies, such as the high-temperature surface reassembly of SiC-decomposed carbons[13−15] and the catalytic chemical vapor deposition (CVD) of hydrocarbons on substrate surfaces,[16−18] have been proven as potential solutions for the aggregation problem of graphene

sheets with an undamaged π-conjugated system. However, the low yield of graphene and the strict conditions limit graphene application in large-scale synthesis.[19] Consequently, determining ways to facilitate the 2D-oriented assembly of carbons into graphene instead of other carbon structures while restraining the $\pi-\pi$ stacking interaction is a challenge for the controllable bulk synthesis of graphene, which is vital both scientifically and technically. Stride and Choucair et al.[20] have successfully synthesized graphene through the low-temperature flash pyrolysis of the solvothermal product of sodium and ethanol. Graphene foam is also synthesized through the combustion of sodium ethoxide obtained through the solvothermal process with sodium and ethanol.[21] During this process, the interaction between two sheets is prevented effectively, and graphene can be obtained in a gram scale. However, the formation
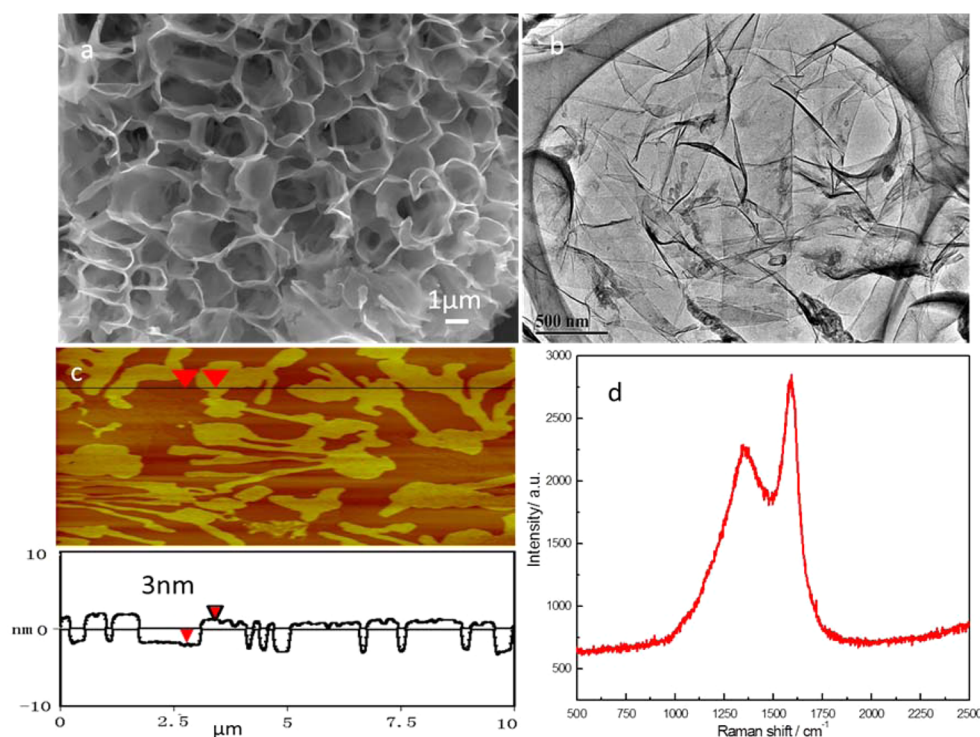
Figure 1. Characterization of GFs synthesized from *n*-propanol and sodium hydroxide. (a,b) SEM and TEM images of GFs. (c) AFM image of GFs. The thickness is about 3 nm for few-layer graphene. (d) Raman spectrum of GFs.

mechanism of graphene and the roles of heat treatment and metal sodium are not presented in detail.

In the present work, graphene frameworks (GFs) were synthesized using common laboratory reagents, namely, *n*-propanol and sodium hydroxide. Remarkably, sodium hydroxide was used instead of sodium, which can certainly decrease risks. More importantly, the mechanism of GFs formation, including the roles of solvothermal and rapid pyrolytic processes, the effects of sodium, and the linkage functions of ether bonds for graphene network formation, was studied systematically and verified by further using acetic acid and sodium hydroxide as initial materials. Furthermore, GFs exhibited high supercapacitor performance as electrode materials, with a specific capacitance of 310.7 F/g at the current density of 0.2 A/g.

■ EXPERIMENTAL SECTION

Synthesis of Graphene Frameworks. A typical synthesis with the solvothermal reaction was performed, consisting of heating sodium hydroxide (3.5 g) and *n*-propanol (8 mL) in a sealed stainless steel reactor at 200 °C for 36 h to yield a solid solvothermal product. Subsequently, a horizontal tubular quartz reactor was preheated to 1000 °C at a rate of 10 °C/min. Next, a combustion boat with the solid solvothermal product (originally laid at the upstream cool zone of the reactor) was shifted to the constant temperature zone to allow the starting materials to decompose at a high heating rate (about 60 °C/s) for 60 s under an argon stream. The resulting black solids were moved out of the high-temperature zone and allowed to gradually cool to room temperature. The remaining product was washed several times with deionized water, and the suspended solid was filtered and oven-dried in a vacuum at 60 °C for 24 h. The synthesis conditions for the other alcohols were similar to those of *n*-propanol. When the carbon source was acetic acid, the temperatures for the solvothermal and pyrolytic processes were 180 and 1150 °C, respectively. The other conditions were consistent with the former. All the chemical reagents

used here were analytical grade and used as received without further treatment.

Sample Characterization. The solvothermal intermediate and GFs morphologies were investigated by scanning electron microscopy (SEM) (JSM-7001F) and high-resolution transmission electron microscopy (HRTEM) (JEM-2100F). Atomic force microscopy (AFM) was performed using a NanoScope IV instrument. Raman measurements were conducted on a LabRAM HR Raman system (514 nm line of an Ar laser as the excitation source). X-ray photoelectron spectrum (XPS) analyses were performed using a Thermo ESCALAB 250 spectrometer (Al−KR X-ray source with a 500 μm electron beam pot). The Fourier-transformed infrared (FTIR) spectrum was obtained using a Tensor 27 infrared spectrometer. Thermogravimetric analysis−mass spectrometry (TGA−MS) was performed using an Evolution 16/18 and an OMNI Star instrument within 10 °C/min to 900 °C under argon protection. Solid nuclear magnetic resonance (NMR) spectra were obtained using an Avance AV 400 spectrometer. X-ray diffraction (XRD) was performed using a Bruker D8 Advance X-ray powder diffractometer with Cu Kα (λ = 1.5406 Å) radiation. The N_2 adsorption and desorption isotherms were measured at 77 K using the ASAP 2020 system (USA).The conductivity of GFs was measured by a Four-Point Probes resistivity measurement system (RTS-9).

Electrochemical Measurements. Working electrodes were fabricated by mixing GFs with acetylene black (10 wt %) and polytetrafluoroethylene binder (5 wt %). The mixture (2 mg) was pressed onto nickel foam current collectors to create electrodes. The prepared electrodes were vacuum-dried at 60 °C for 10 h. Before electrochemical testing, the electrodes were soaked overnight in electrolyte. Electrochemical tests were performed in aqueous 6 M KOH electrolyte with a three-electrode system in which platinum was the counter electrode and Hg−HgCl$_2$ was the reference electrode. The electrochemical performances were characterized by cyclic voltammetry (CV) and galvanostatic charge and discharge measurements. CV was conducted at an electrochemical workstation (CHI660D). Galvanostatic tests were performed using a galvanostatic charge and discharge device (LAND CT2001A).
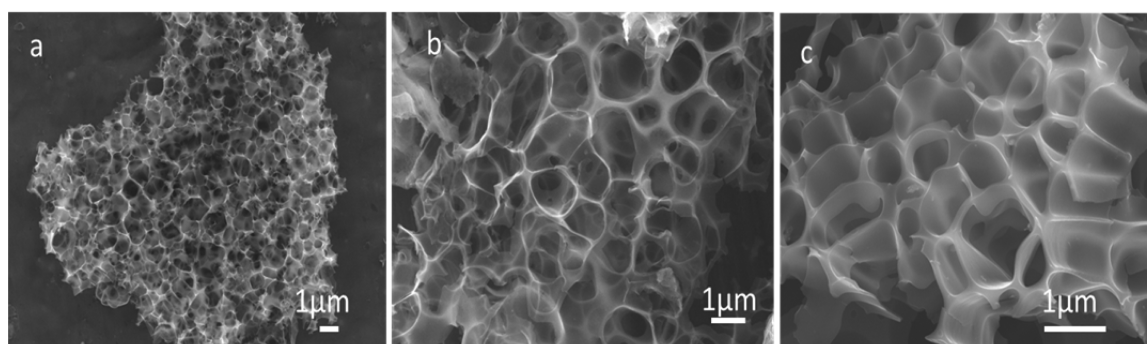
Figure 2. SEM images of GFs synthesis based on different alcohol sources and sodium hydroxide: (a) methanol, (b) ethanol, and (c) 1,4-butanediol.
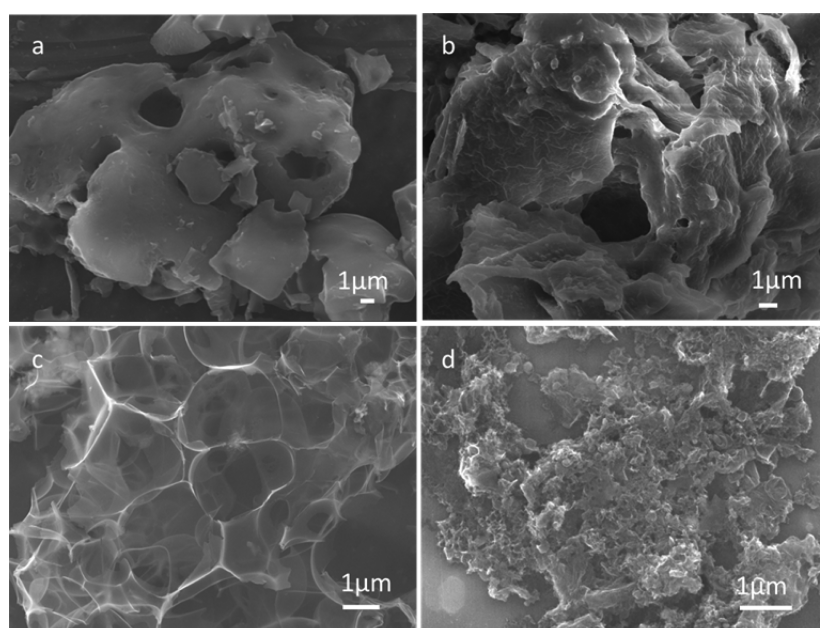

Figure 3. SEM images of different products. (a) Direct pyrolysis product of sodium ethoxide solid. (b) Solvothermal product of *n*-propanol and sodium hydroxide. (c) Pyrolysis product of ethanol with sodium ethoxide. (d) Pyrolysis product via temperature programming.

■ RESULTS AND DISCUSSION

Figure 1 shows the characterization results for GFs obtained after the pyrolysis of the solvothermal products of *n*-propanol and sodium hydroxide. Pure 3D networks constructed with graphene sheets were evident in the SEM (Figure 1a) and TEM (Figure 1b) images. Few-layer graphene was confirmed with a thickness of 3 nm, as measured by AFM (Figure 1c). The Raman spectrum is shown in Figure 1d, and the G-band at 1586 cm^{-1} demonstrates the formation of graphitic carbon.[22] Excluding *n*-propanol, other alcohols (such as methanol, ethanol, and butanediol) can also be used to produce graphene, which suggests a generality of the method of graphene synthesis (Figures 2 and S1 in the Supporting Information). Given that sodium hydroxide was used instead of sodium, the development process became much safer and easier.

To understand the formation mechanism of GFs, we investigated their development processes. Because alcohol and sodium hydroxide can react to form sodium alcoholate (Figure S2 in the Supporting Information), purchased sodium ethoxide solid (instead of the solvothermal product of alcohol–sodium hydroxide) was used to carry through the pyrolysis. Figure 3a shows the morphology and structure of the pyrolysis powders. A stacking bulk structure instead of a sheet structure

was obtained, which clearly indicated that graphene cannot be synthesized through the direct pyrolysis of sodium ethoxide solids. To study the roles of the solvothermal processes, we analyzed the morphology and structure of solvothermal intermediates. Figure 3b evidently shows the number of cavities and pores, which may trap unreacted alcohol and enhance graphene formation after a quick pyrolysis. The pore size distribution of the solvothermal intermediates was further confirmed by the measurement of N$_2$ adsorption and desorption, which showed two obvious pore distributions at 10−100 and 3−4 nm (Figure S3 in the Supporting Information). To ensure the existence of unreacted alcohol, we analyzed the solvothermal intermediates by TGA−MS, as shown in Figure S4 in the Supporting Information. At about 120 °C, an obvious weight loss position was found, accounting for nearly 50% of its original weight (Figure S4a, Supporting Information). Together with the result from the MS (Figure S4b, Supporting Information), it can be confirmed that the weight loss was due to the volatilization of H$_2$O and *n*-propanol. The apparent signal of *n*-propanol (Figure S4b in the Supporting Information) suggests that large amounts of *n*-propanol were existent in the solvothermal product. This analysis can also be confirmed by the TGA−MS results for the solvothermal product of ethanol and sodium hydroxide (parts c
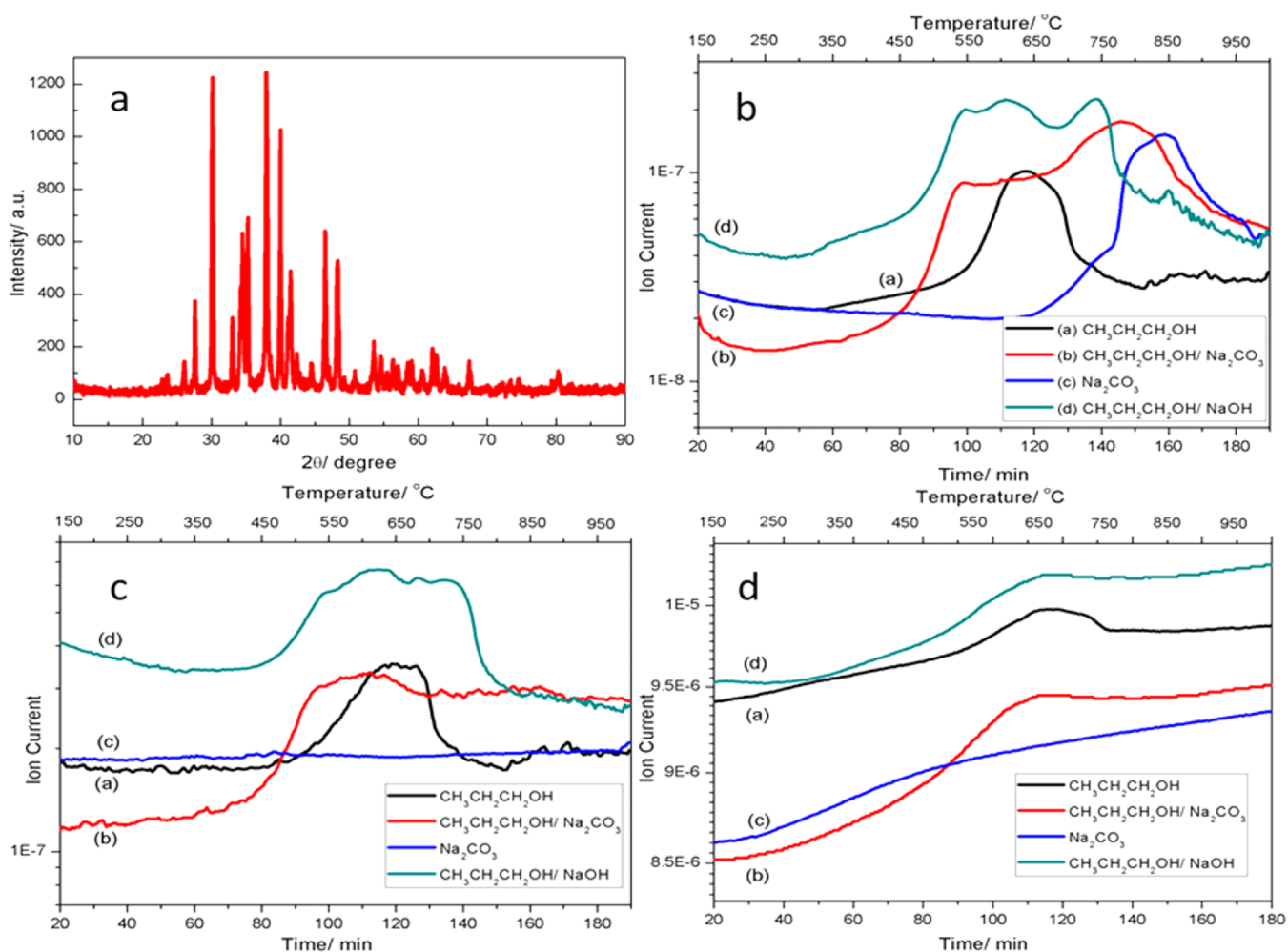
Figure 4. (a) X-ray diffraction pattern of as-prepared GFs obtained from the rapid decomposition of the solvothermal products of *n*-propanol and sodium hydroxide at 1000 °C. Detected MS signals: (b) CO_2, (c) H_2O, and (d) CO via floating CVD.
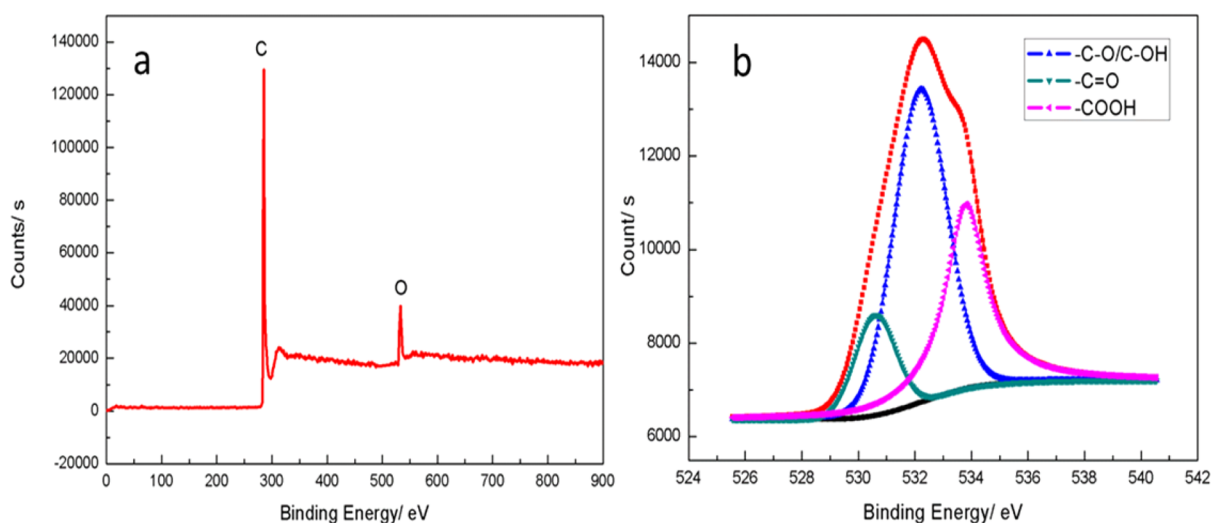

Figure 5. (a) XPS survey spectrum of GFs. (b) O_{1s} spectrum of GFs.

and d of Figures S4 in the Supporting Information). In addition, the speculation was also verified by the observation that GFs can be synthesized by using sodium ethoxide and ethanol as raw materials and following similar solvothermal and rapid pyrolytic processes (Figure 3c). A precursor of the porous

structure of sodium alcoholate and alcohol was formed during the solvothermal process, and the alcohol in this structure played a significant role in the graphene formation during rapid pyrolysis. To analyze the role of rapid pyrolysis, we treated the solvothermal product with temperature programming. The
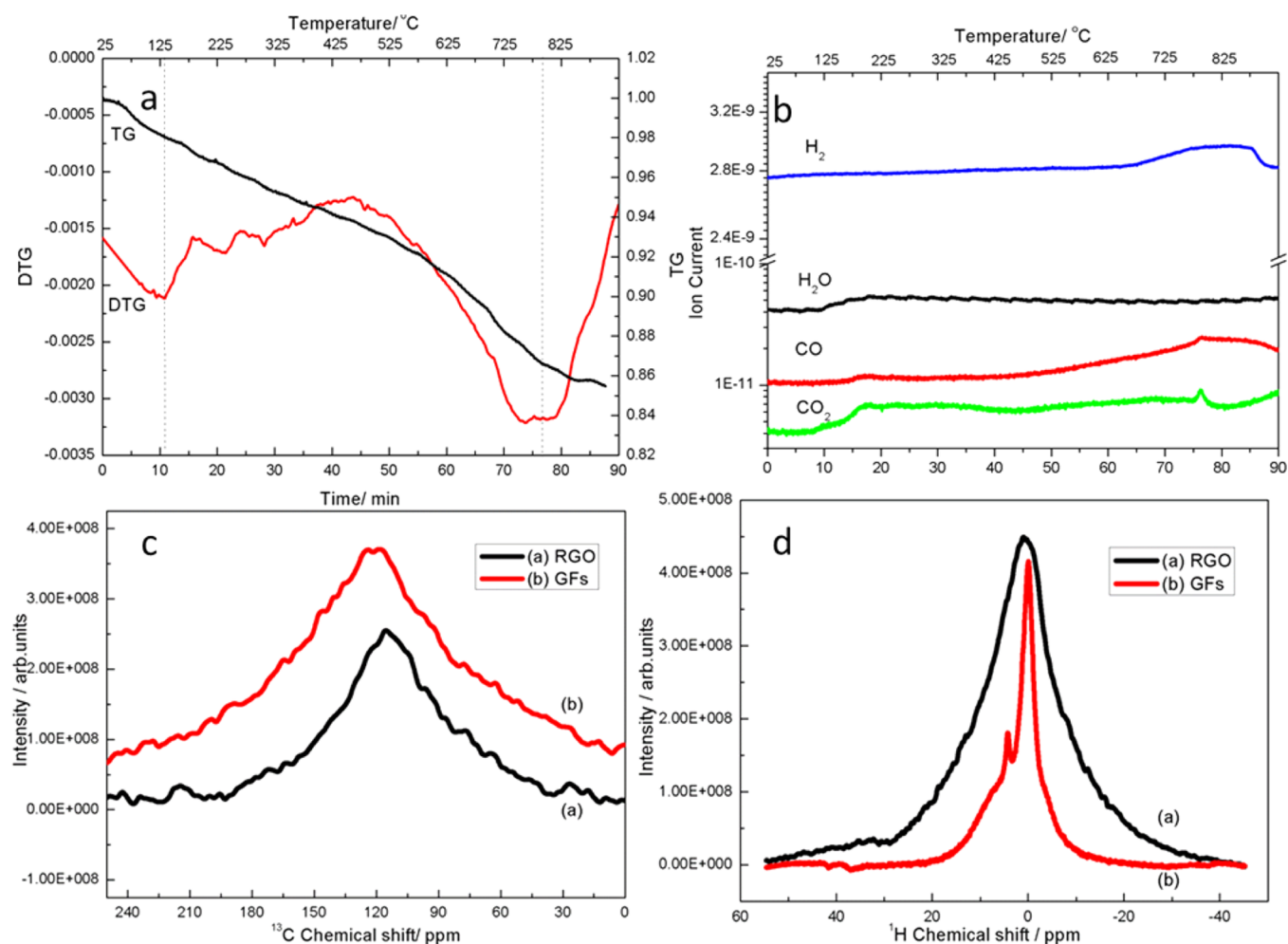
Figure 6. (a) TGA curves and (b) MS signals of detected H_2, H_2O, CO_2, and CO. (c) Solid ^{13}C NMR and (d) relevant ^1H NMR spectra of GFs.

relevant morphologies and structures are displayed in Figure 3d. When these are compared with the SEM image in Figure 1a, it is clear that GFs cannot be formed through temperature programming pyrolysis. The instantaneous high inner pressure generated during rapid pyrolysis is important in graphene formation. When the pressure is high enough, the stack can be effectively restrained during the self-assembly of carbon atoms, which leads to the formation of graphene instead of graphite.

Sodium-containing compounds, used as a catalyst in coal gasification, can enhance the reaction potential and weaken the C−O bond to improve the gasification reaction rate and promote carbon conversion.[23−25] Catalyzing the decomposition and gasification of the solvothermal intermediate during rapid pyrolysis is easy for the remaining sodium in the solvothermal product. Mass spectrometry (MS) was used to detect gases produced by floating CVD to analyze the role of sodium (see the Supporting Information). The XRD result (Figure 4a) showed that sodium carbonate (PDF: 37−0451) was formed during fast pyrolysis; thus, sodium carbonate was selected as the sodium source for the contrast experiments. (Metallic Na, which may play a role in the process, may be produced in situ when the furnace temperature is around 1000 °C. This guess will be studied in the further work.) Figure 4b−d showed the MS spectra results, including the signals of carbon dioxide, water, and carbon monoxide. All these signals obviously occurred earlier when sodium was present. Among these signals, those of water and carbon dioxide occurred about 20

min earlier and at temperatures about 100 °C lower than the decomposition and gasification temperatures of *n*-propanol without Na_2CO_3. In addition, the result of the NaOH and *n*-propanol system was also tested and was similar to that of the Na_2CO_3 and *n*-propanol system. These findings suggested that sodium-containing materials can enhance the decomposition and gasification of solvothermal products during rapid pyrolysis.

The elemental composition and binding configurations of GFs were investigated via XPS and FTIR measurements (Figures 5 and S6 in the Supporting Information). The XPS survey spectrum showed a dominant narrow graphitic C_{1s} peak at 284 eV and a weak O_{1s} peak at ∼532 eV (Figure 5a). The atomic percentage of the O element is about 10%, suggesting the presence of some oxygen functional groups. The main peak that existed at 532.4 eV was evident in the high-resolution O_{1s} spectrum (Figure 5b), which suggested that C−O−C and C−OH dominated the 3D graphene.[11,26] This result was consistent with the high-resolution C_{1s} spectrum (Figure S5, Supporting Information). The FTIR spectrum (Figure S6, Supporting Information) consistently displayed an obvious peak at ∼1200 cm^{-1}, which referred to the stretching vibration of C−O−C and C−OH.[21,27] Because the peak at ∼3300 cm^{-1} corresponding to O−H was quite weak, it may imply that GFs contains fewer O−H bonds.

To further understand the oxygen configuration, we characterized the GFs by TGA−MS (panels a and b of Figure
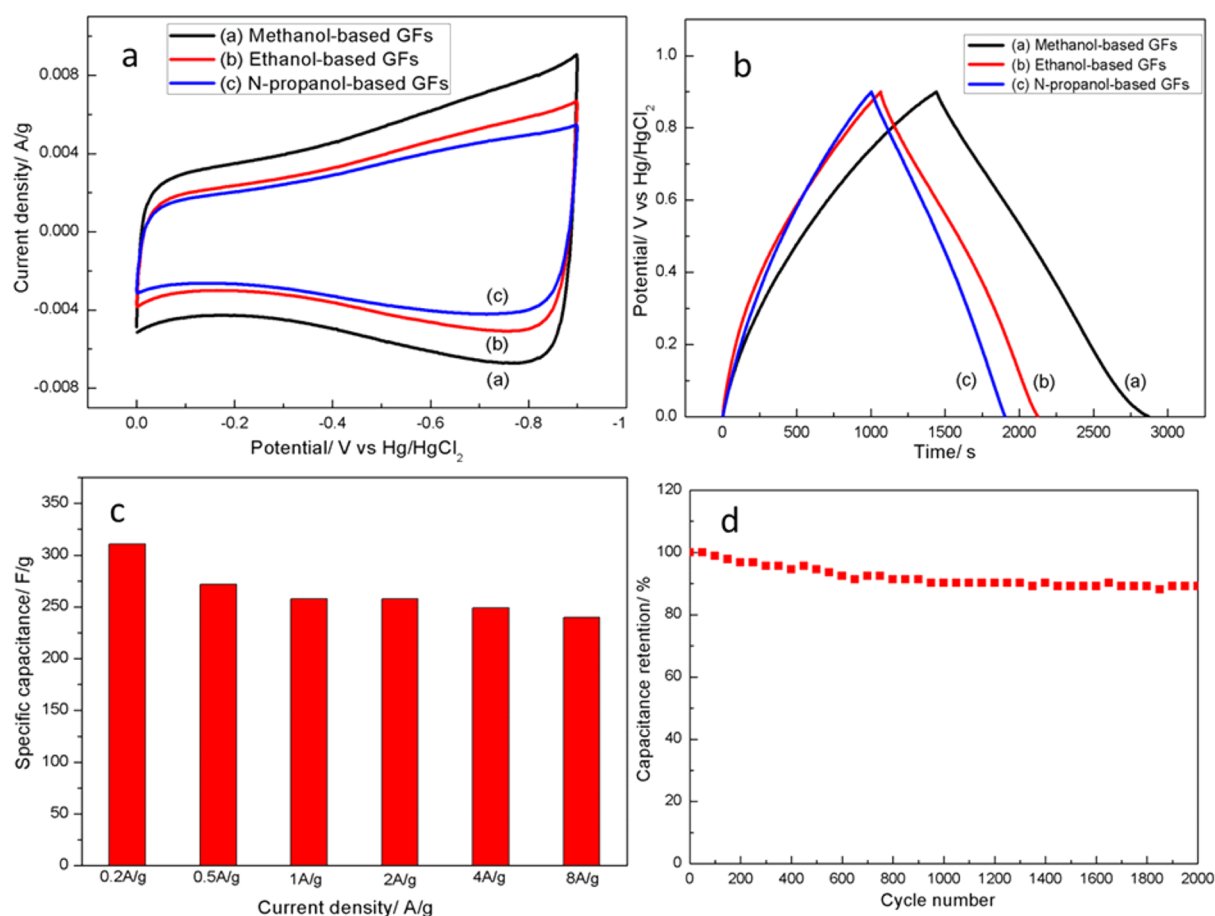
Figure 7. Capacitive performance of GFs-modified electrodes in 6 M KOH aqueous solution with a three-electrode system. (a) CV curves at a scan rate of 30 mV/s. (b) Galvanostatic charge and discharge curves at a current density of 0.2 A/g. (c) Column graph of capacitance of the methanol-based GFs electrode obtained at various current densities. (d) Cycle stability of the methanol-based GFs electrode at a current density of 2 A/g.

6). There were two apparent weight loss positions found after 10 and 76 min (Figure 6a), separately. When these data are compared with the MS data (Figure 6b), it is clear that the weight loss at 10 min (about 130 °C) resulted from the desorption of the physical adsorption of H_2O,[28] whereas the weight loss at 76 min (about 780 °C) was associated with oxygen and hydrogen elimination in the defects. Considering that the mainly released gas was CO instead of H_2O, the C−O−C content may be greater than that of C−OH. Previous reports have shown that materials containing C−O−C can form CO via hydrogen atom migration.[29,30] Because the signal of H_2 was also quite obvious, which may result from the release of the H atom in the graphene edges or defects or the decomposition of H_2O, the lessened H_2O signal and increased CO signal may be due to the reaction of H_2O and C. Therefore, the conclusion should be verified by further evidence.

The results were further confirmed by the solid-state ^{13}C and ^{1}H NMR of GFs and reduced graphene oxide (RGO); the synthesis process of RGO is presented in the Supporting Information. Figure 6c shows the ^{13}C NMR spectra of the two kinds of graphene. Both spectra showed a dominant peak at ~120 ppm that was attributed to the sp^2 carbon.[31,32] However, a significant difference existed between the ^{1}H NMR spectra of the two kinds of graphene: a distinct peak emerged at ~4 ppm in the GFs, resulting from the ether bond (Figure 6d).[33] As mentioned above, 3D graphene contained abundant C−O−C. Given that the C−O−C bond is sp^3 hybridized, and the bond

angle is ~110°, constructing a 3D framework structure is easier than developing a sp^2 hybridized C=C bond.

On the basis of the above analysis, the evolution mechanism of the GFs can be summarized as follows. In the solvothermal process, a precursor of a porous structure was initially formed. The occluded organics were either volatile or labile, which can generate instantaneous high internal pressure during rapid pyrolysis. Under high temperature and sodium catalysis, the precursors rapidly decomposed to produce abundant carbon atoms, which then self-assembled to form graphene. With the linkage of numerous ether bonds, the as-grown graphene formed a 3D framework structure. Theoretically, materials that can form an oxygen-enriched porous precursor can possibly synthesize GFs, which should not be confined to alcohols. This finding has been verified, given that GFs can be synthesized using acetic acid and sodium hydroxide as raw materials (Figures S7 and S8 in the Supporting Information).

When compared with the graphene frameworks fabricated with other methods,[34−36] some differences in the detailed structure and macroscopic properties of GFs can be observed. The 3D macroporous bubble graphene film was obtained by a hard template-directed ordered assembly approach, during which the graphene oxide precursor and template poly(methyl methacrylate) spheres were assembled in an ordered approach by vacuum filtration and calcinated to reduce the graphene oxide into graphene.[34] With an average pore diameter of 107.3 nm, the macroporous structure's size is smaller than the GFs

synthesized by our methods (about 1−3 μm, Figure 1a). The larger macroporous structure may reserve more electrolytes to reduce the diffusion length and therefore improve the rate capacity of electrochemical devices such as supercapacitors. Self-assembled foamlike graphene structures were formed using a nucleate boiling method,[35] in which the self-assembly of RGO platelets occurred through condensation or hydrogen bonding. Compared with the chemical bond joints (C−O−C) in our method, these interaction forces are weaker, which may lead to a poorer mechanical stability of the framework structure. The 3D graphene networks can also be synthesized by chemical vapor deposition.[36] The obtained graphene with this kind of method has little defects; therefore, it is quite suitable for the application in field effect transistor.[18] However, the wettability of this kind of graphene is poor, especially in aqueous solution, which is unfavorable to apply in electrode materials. The presence of some oxygen-containing functional groups in graphene can enhance the wettability effectively.

Because the synthesized graphene exhibited a framework structure, it can effectively restrain the $\pi-\pi$ stacking interaction and allow electrolytes to freely diffuse inside and through the network,[35,37,38] relatively benefiting the supercapacitor application. The capacitive performance of GFs was then investigated by CV and galvanostatic charge and discharge measurements. As shown in Figure 7a, all of the CV curves of the GFs-modified electrodes measured in 6 M KOH aqueous solution with a three-electrode system have rectangular shapes at the scan rate of 30 mV/s, which reveals the good charge storage capacity of the GFs materials. Figure 7b shows the galvanostatic charge and discharge curves of different GFs-modified electrodes. The specific capacitances of methanol-, ethanol-, and n-propanol-based GFs-modified electrodes were 310.7, 235.1, and 188.4 F/g, respectively, at 0.2 A/g. The higher specific capacitance of the methanol-based GFs-modified electrode may be attributed to the larger BET specific surface area (748.7, 539.6, and 178.7 m^2/g for methanol-, ethanol-, and n-propanol-based GFs, respectively), which can adsorb more electrolyte ions for capacitance formation. Given the high oxygen content of methanol, more gases were produced from methanol to restrict the restacking behavior during the formation of GFs, which can generate a larger specific surface area. Except for the high specific capacitance, methanol-based GFs-modified electrode also demonstrated an excellent rate capability. At a high rate of 8 A/g, the electrode maintained a specific capacitance of 240 F/g with a retention rate of 77% (Figure 7c). The excellent rate capability may be ascribed to the good conductivity (44 S/m for methanol-based GFs) and framework characteristics of GFs, which can provide multi-electron and ion transport channels when methanol-based GFs-modified electrodes serve as electrode materials. In addition, the cycle life of methanol-based GFs-modified electrodes was also measured, as shown in Figure 7d. The methanol-based GFs exhibit good cycle stability and can retain over 90% of its capacitance over 2000 cycles at a current density of 2 A/g.

Compared with graphene materials synthesized by other methods,[34,37,39−41] the GFs synthesized by our method also displays better electrochemistry supercapacitor performance (Table S1, Supporting Information). The larger specific capacitance of GFs may be due to the synergistic effects of several factors. First, the large specific surface area can absorb more electrolyte ions to construct capacitance. Second, the presence of some oxygen-containing functional groups can offer a good wettability of graphene materials to electrolyte ions and therefore enhance the construction of capacitance. Third, the well-constructed framework structure may reserve more electrolytes to reduce the diffusion length and offer multiple electrons and ions transport routes, which can improve the performance of the supercapacitor effectively.

CONCLUSIONS

GFs were synthesized with the alcohol−sodium hydroxide system through the solvothermal and rapid pyrolysis processes. Notably, the evolution mechanism of GFs was investigated systematically. Several synergistic factors existed in the formation of GFs. In the solvothermal process, a precursor of a porous oxygen-enriched structure was formed, which then generated the instantaneous high internal pressure during rapid pyrolysis. Under sodium catalysis, the abundant carbon atoms produced from the decomposition of the precursors self-assembled to form graphene. The existence of abundant ether bonds may be favorable for the formation of 3D graphene. Furthermore, GFs were also successfully obtained using acetic acid as a carbon source in the synthetic process, suggesting the reasonability of analyzing the formation mechanism. Determining more favorable routes by which to synthesize graphene under this cognition will be quite possible, which is extremely important for the large-scale synthesis and wide application of graphene. Furthermore, the electrochemical energy storage capacity of GFs was studied, and an excellent supercapacitor performance with a specific capacitance of 310.7 F/g at a current density of 0.2 A/g was found in GFs.

ASSOCIATED CONTENT

Ⓢ Supporting Information

Details of the synthesis process of RGO and the experimental equipment designed to investigate the role of sodium; figures showing the Raman, C1s, and FTIR spectra of GFs; figures showing the XRD patterns, pore size distribution, and TGA−MS analysis of solvothermal product; an SEM image of GFs synthesized by the rapid pyrolysis of solvothermal products of acetic acid and sodium hydroxide; and a table showing the comparison of specific capacitance between this work and other carbon materials are presented. The Supporting Information is available free of charge on the ACS Publications website at DOI: 10.1021/acsami.5b01201.

AUTHOR INFORMATION

Corresponding Authors
*E-mail: zhengjf@sxicc.ac.cn.
*E-mail: zpzhu@sxicc.ac.cn.

Author Contributions
The manuscript was written through contributions of all authors. All authors have given approval to the final version of the manuscript.

Notes
The authors declare no competing financial interest.

REFERENCES

(1) Luo, B.; Liu, S.; Zhi, L. Chemical Approaches Toward Graphene-Based Nanomaterials and Their Applications in Energy-Related Areas. *Small* **2012**, *8*, 630−646.

(2) Jiang, H. Chemical Preparation of Graphene-Based Nanomaterials and Their Applications in Chemical and Biological Sensors. *Small* **2011**, *17*, 2413−2427.

(3) Wang, H.; Maiyalagan, T.; Wang, X. Review on Recent Progress in Nitrogen-Doped Graphene: Synthesis, Characterization, and Its Potential Applications. *ACS Catal.* **2012**, *5*, 781−794.

(4) Ning, G.; Fan, Z.; Wang, G.; Gao, J.; Qian, W.; Wei, F. Gram-Scale Synthesis of Nanomesh Graphene with High Surface Area and Its Application in Supercapacitor Electrodes. *Chem. Commun. (Cambridge, U. K.)* **2011**, *47*, 5976−5978.

(5) Dong, L.; Chen, Z.; Yang, D.; Lu, H. Hierarchically Structured Graphene-Based Supercapacitor Electrodes. *RSC Adv.* **2013**, *3*, 21183−21191.

(6) Zhang, X.; Zhang, H.; Li, C.; Wang, K.; Sun, X.; Ma, Y. Recent Advances in Porous Graphene Materials for Supercapacitor Applications. *RSC Adv.* **2014**, *4*, 45862−45884.

(7) Singh, V.; Joung, D.; Zhai, L.; Das, S.; Khondaker, S. I.; Seal, S. Graphene Based Materials: Past, Present and Future. *Prog. Mater. Sci.* **2011**, *56*, 1178−1271.

(8) Maschmann, M. R.; Franklin, A. D.; Sands, T. D.; Fisher, T. S. Optimization of Carbon Nanotube Synthesis from Porous Anodic Al−Fe−Al Templates. *Carbon* **2007**, *45*, 2290−2296.

(9) Takehara, H.; Fujiwara, M.; Arikawa, M.; Diener, M. D.; Alford, J. M. Experimental Study of Industrial Scale Fullerene Production by Combustion Synthesis. *Carbon* **2005**, *43*, 311−319.

(10) Presser, V.; Heon, M.; Gogotsi, Y. Carbide-Derived Carbons-From Porous Networks to Nanotubes and Graphene. *Adv. Funct. Mater.* **2011**, *21*, 810−833.

(11) Quintana, M.; Grzelczak, M.; Spyrou, K.; Calvaresi, M.; Bals, S.; Kooi, B.; Van Tendeloo, G.; Rudolf, P.; Zerbetto, F.; Prato, M. A Simple Road for the Transformation of Few-Layer Graphene into MWNTs. *J. Am. Chem. Soc.* **2012**, *134*, 13310−13315.

(12) Zhang, W.; Cui, J.; Tao, C. A.; Wu, Y.; Li, Z.; Ma, L.; Wen, Y.; Li, G. A Strategy for Producing Pure Single-Layer Graphene Sheets Based on a Confined Self-Assembly Approach. *Angew. Chem., Int. Ed.* **2009**, *48*, 5864−5868.

(13) Hite, J. K.; Twigg, M. E.; Tedesco, J. L.; Friedman, A. L.; Myers-Ward, R. L.; Eddy, C. R.; Gaskill, D. K. Epitaxial Graphene Nucleation on C-Face Silicon Carbide. *Nano Lett.* **2011**, *11*, 1190−1194.

(14) Robinson, J.; Weng, X.; Trumbull, K.; Cavalero, R.; Wetherington, M.; Frantz, E.; LaBella, M.; Hughes, Z.; Fanton, M.; Snyder, D. Nucleation of Epitaxial Graphene on SiC(0001). *ACS Nano* **2009**, *4*, 153−158.

(15) Berger, C.; Song, Z.; Li, T.; Li, X.; Ogbazghi, A. Y.; Feng, R.; Dai, Z.; Marchenkov, A. N.; Conrad, E. H.; First, P. N. Ultrathin Epitaxial Graphite: 2D Electron Gas Properties and a Route Toward Graphene-Based Nanoelectronics. *J. Phys. Chem. B* **2004**, *108*, 19912−19916.

(16) Somani, P. R.; Somani, S. P.; Umeno, M. Planer Nano-graphenes from Camphor by CVD. *Chem. Phys. Lett.* **2006**, *430*, 56−59.

(17) Li, X.; Magnuson, C. W.; Venugopal, A.; Tromp, R. M.; Hannon, J. B.; Vogel, E. M.; Colombo, L.; Ruoff, R. S. Large-Area Graphene Single Crystals Grown by Low-Pressure Chemical Vapor Deposition of Methane on Copper. *J. Am. Chem. Soc.* **2011**, *133*, 2816−2819.

(18) Li, X.; Cai, W.; An, J.; Kim, S.; Nah, J.; Yang, D.; Piner, R.; Velamakanni, A.; Jung, I.; Tutuc, E.; Banerjee, S. K.; Colombo, L.; Ruoff, R. S. Large-Area Synthesis of High-Quality and Uniform Graphene Films on Copper Foils. *Science* **2009**, *324*, 1312−1314.

(19) Weiss, N. O.; Zhou, H.; Liao, L.; Liu, Y.; Jiang, S.; Huang, Y.; Duan, X. Graphene: an Emerging Electronic Material. *Adv. Mater.* **2012**, *24*, 5782−5825.

(20) Choucair, M.; Thordarson, P.; Stride, J. A. Gram-Scale Production of Graphene Based on Solvothermal Synthesis and Sonication. *Nat. Nanotechnol.* **2009**, *4*, 30−33.

(21) Lyth, S. M.; Shao, H.; Liu, J.; Sasaki, K.; Akiba, E. Hydrogen Adsorption on Graphene Foam Synthesized by Combustion of Sodium Ethoxide. *Int. J. Hydrogen Energy* **2014**, *39*, 376−380.

(22) Zhou, D.; Cheng, Q. Y.; Han, B. H. Solvothermal Synthesis of Homogeneous Graphene Dispersion with High Concentration. *Carbon* **2011**, *49*, 3920−3927.

(23) Van Eyk, P. J.; Ashman, P. J.; Nathan, G. J. Mechanism and Kinetics of Sodium Release from Brown Coal Char Particles during Combustion. *Combust. Flame* **2011**, *158*, 2512−2523.

(24) Wu, L.; Qiao, Y.; Gui, B.; Wang, C.; Xu, J.; Yao, H.; Xu, M. Effects of Chemical Forms of Alkali and Alkaline Earth Metallic Species on the Char Ignition Temperature of a Loy Yang Coal under O_2/N_2 Atmosphere. *Energy Fuels* **2012**, *26*, 112−117.

(25) Kuang, H. P.; Zhou, J. H.; Zhou, Z. J.; Liu, H. Z.; Cen, K. F. Catalytic Mechanism of Sodium Compounds in Black Liquor During Gasification of Coal Black Liquor Slurry. *Energy Convers. Manage.* **2008**, *49*, 247−256.

(26) Larciprete, R.; Fabris, S.; Sun, T.; Lacovig, P.; Baraldi, A.; Lizzit, S. Dual Path Mechanism in the Thermal Reduction of Graphene Oxide. *J. Am. Chem. Soc.* **2011**, *133*, 17315−17321.

(27) Pham, V. H.; Cuong, T. V.; Hur, S. H.; Oh, E.; Kim, E. J.; Shin, E. W.; Chung, J. S. Chemical Functionalization of Graphene Sheets by Solvothermal Reduction of a Graphene Oxide Suspension in *N*-Methyl-2-pyrrolidone. *J. Mater. Chem.* **2011**, *21*, 3371−3377.

(28) Kuila, T.; Mishra, A. K.; Khanra, P.; Kim, N. H.; Uddin, M. E.; Lee, J. H. Facile Method for the Preparation of Water Dispersible Graphene Using Sulfonated Poly(ether−ether−ketone) and Its Application as Energy Storage Materials. *Langmuir* **2012**, *28*, 9825−9833.

(29) Tsujino, Y.; Yasaka, Y.; Matubayasi, N.; Nakahara, M. Pathways and Kinetics of Anisole Pyrolysis Studied by NMR and Selective 13C Labeling. Heterolytic Carbon Monoxide Generation. *Bull. Chem. Soc. Jpn.* **2012**, *85*, 124−132.

(30) Lifshitz, A.; Tamburu, C.; Shashua, R. Decomposition of 2-Methylfuran: Experimental and Modeling Study. *J. Phys. Chem. A* **1997**, *101*, 1018−1029.

(31) Gao, W.; Alemany, L. B.; Ci, L.; Ajayan, P. M. New Insights into the Structure and Reduction of Graphite Oxide. *Nat. Chem.* **2009**, *1*, 403−408.

(32) Cai, W.; Piner, R. D.; Stadermann, F. J.; Park, S.; Shaibat, M. A.; Ishii, Y.; Yang, D.; Velamakanni, A.; An, S. J.; Stoller, M. Synthesis and Solid-State NMR Structural Characterization of 13C-Labeled Graphite Oxide. *Science* **2008**, *321*, 1815−1817.

(33) Hu, Z.; Fan, X.; Wang, J.; Zhao, S.; Han, X. A Facile Synthesis of Hydrophilic Glycopolymers with the Ether Linkages throughout the Main Chains. *J. Polym. Res.* **2010**, *17*, 815−820.

(34) Chen, C. M.; Zhang, Q.; Huang, C. H.; Zhao, X. C.; Zhang, B. S.; Kong, Q. Q.; Wang, M. Z.; Yang, Y. G.; Cai, R.; Sheng Su, D. Macroporous 'Bubble' Graphene Film via Template-Directed Ordered-Assembly for High Rate Supercapacitors. *Chem. Commun.* **2012**, *48*, 7149−7151.

(35) Ahn, H. S.; Jang, J.-W.; Seol, M.; Kim, J. Min; Yun, D.-J.; Park, C.; Kim, H.; Youn, D. H.; Kim, J. Y.; Park, G.; Park, S. C.; Kim, J. Man; Yu, D. I.; Yong, K.; Kim, M. H.; Lee, J. S. Self-Assembled Foam-like Graphene Networks Formed Through Nucleate Boiling. *Sci. Rep.* **2013**, *1396*, 1−8.

(36) Chen, Z.; Ren, W.; Gao, L.; Liu, B.; Pei, S.; Cheng, H. M. Three-Dimensional Flexible and Conductive Interconnected Graphene Networks Grown by Chemical Vapour Deposition. *Nat. Mater.* **2011**, *10*, 424−428.

(37) Wu, Z. S.; Sun, Y.; Tan, Y. Z.; Yang, S.; Feng, X.; Mullen, K. Three-Dimensional Graphene-Based Macro- and Mesoporous Frameworks for High-Performance Electrochemical Capacitive Energy Storage. *J. Am. Chem. Soc.* **2012**, *134*, 19532−19535.

(38) Jiang, X.; Yang, X.; Zhu, Y.; Shen, J.; Fan, K.; Li, C. In Situ Assembly of Graphene Sheets-Supported SnS_2 Nanoplates into 3D Macroporous Aerogels for High-Performance Lithium Ion Batteries. *J. Power Sources* **2013**, *237*, 178−186.

(39) Chen, C. M.; Zhang, Q.; Zhao, X. C.; Zhang, B.; Kong, Q. Q.; Yang, M.-G.; Yang, Q. H.; Wang, M. Z.; Yang, Y. G.; Schlögl, R.; Su, D. S. Hierarchically Aminated Graphene Honeycombs for Electrochemical Capacitive Energy Storage. *J. Mater. Chem.* **2012**, *22*, 14076−14084.

(40) Sun, D.; Yan, X.; Lang, J.; Xue, Q. High Performance Supercapacitor Electrode Based on Graphene Paper via Flame-Induced

Reduction of Graphene Oxide Paper. *J. Power Sources* **2013**, *222*, 52–58.

(41) Yoon, J. C.; Lee, J. S.; Kim, S. I.; Kim, K. H.; Jang, J. H. Three-Dimensional Graphene Nano-networks with High Quality and Mass Production Capability via Precursor-Assisted Chemical Vapor Deposition. *Sci. Rep.* **2013**, *1788*, 1–8.